Available online at www.sciencedirect.com
ScienceDirect
Journal of Hazardous Materials 144 (2007) 406–411
Journal of Hazardous Materials
www.elsevier.com/locate/jhazmat

Thermodynamics and kinetics of adsorption of Cu(II) onto waste iron oxide

Yao-Hui Huang *, Chan-Li Hsueh, Hui-Pin Cheng, Liang-Chih Su, Chuh-Yung Chen

Department of Chemical Engineering, National Cheng Kung University, Tainan City 701, Taiwan

Received 7 June 2006; received in revised form 13 October 2006; accepted 17 October 2006
Available online 26 October 2006

Abstract

This study investigates low-cost sorbents as replacements for current costly methods of removing heavy metals from solution. This investigation explores the waste iron oxide material (F1), which is a by-product of the fluidized-bed reactor (FBR)–Fenton reaction, for use in the treatment of the wastewater in Taiwan. X-ray powder diffraction (XRD) and scanning electron microscopy (SEM) were used to characterize the F1. In this investigation, F1 are tested as adsorbents for removing copper (Cu^{2+}) from aqueous solutions. The highest Cu^{2+} adsorption capacity of F1 adsorbent was determined as 0.21 mmol g^{-1} for 0.8 mmol dm^{-3} initial Cu^{2+} concentration at pH 6.0 and 300 K. Adsorption data were well described by the Freundlich model and the thermodynamic constants of the adsorption process, ΔG°, ΔH° and ΔS° were evaluated as -6.12 kJ mol^{-1} (at 318 K), 9.2 kJ mol^{-1} and 48.19 J mol^{-1} K^{-1} (at 318 K), respectively. Additionally, a pseudo-second-order rate model was adopted to describe the kinetics of adsorption.

Keywords: Adsorption; Iron oxide; Copper; Thermodynamic; Kinetics

1. Introduction

Heavy metals in water have been a major preoccupation for many years because of their toxicity towards aquatic life, human beings and the environment. As they do not degrade biologically like organic pollutants [1], their presence in industrial effluents or drinking water is a public health problem due to their absorption and therefore possible accumulation in organisms. Copper (Cu^{2+}) is of particular interest because of its toxicity and its widespread presence in the industrial applications, e.g. electrical, electro-plating, metal-finishing and paint industries. The toxicity of copper may cause itching and dermatitis, keratinization of the hands, and the soles of the feet [2]. Therefore, the concentrations of these metals must be reduced to levels that satisfy environmental regulations for various bodies of water.

Several techniques are available for removing heavy metals from aqueous solutions. They include chemical precipitation, conventional coagulation, reverse osmosis, ion exchange and adsorption. One of these techniques, the adsorption method, is simple and cost-effective, and is extensively adopted [3–5]. Adsorption onto activated carbon has proven to be one of the most effective and reliable physicochemical treatment methodologies [6–11]. However, commercially available activated carbons are very expensive. Babel and Kurniawan [12] and Bailey et al. [13] have presented interesting reviews of the potential of a wide range of low-cost sorbents of heavy metals. According to these researchers, a sorbent can be assumed to be low-cost if it requires little prior processing, is naturally abundant, or is either a by-product or a waste material from another industry. These materials may represent alternatives to expensive treatment processes.

Recently, interest in low-cost, high-surface-area materials, especially metal oxides, and their unique applications, such as adsorption and chemical catalysis, has been growing. Iron oxide has a relatively high surface area and charge; numerous researchers have used iron oxide as an adsorbent to treat heavy metals and organic compounds from wastewater [14–18]. This study elucidates the F1 adsorbent, which is from the FBR–Fenton process [19,20], for use in treating wastewater from dyeing/finishing plants in Taiwan. This process not only provides a high COD removal efficiency but also reduces the large

* Corresponding author. Tel.: +886 6 2757575x62636; fax: +886 6 2344496.
E-mail address: yhhuang@ccmail.ncku.edu.tw (Y.-H. Huang).

0304-3894/$ – see front matter © 2006 Elsevier B.V. All rights reserved.
doi:10.1016/j.jhazmat.2006.10.061

amount of Fe sludge produced [19]. However, the iron oxide must be taken out from the FBR after an extended reaction; meanwhile, repacked activated alumina supports for fluidizing. The iron oxide, which is a by-product of the FBR–Fenton process, becomes waste. Hence, it is important to find the other application of the waste iron oxide for the recycling of waste. In our earlier investigation [21], the sinter of F1 (denoted as FeAA-500) was successfully applied as a heterogeneous photooxidative catalyst of the degradation azo dye. In this work, the tests and uses of the iron oxide as adsorbents for the removal of copper (Cu^{2+}) from aqueous solutions are carried out further.

This work examines the thermodynamics and kinetics of the adsorption of Cu^{2+} by an adsorbent, to evaluate the thermodynamic parameters; establish the adsorption rate equation, and assess the effectiveness of iron oxide as an adsorbent of heavy metals from wastewater. The experimental data were fitted to Langmuir and Freundlich equations, to determine which isotherm most closely correlates with experimental data. The first-order Lagergren, pseudo-second-order and second-order equations were adopted to test the experimental data.

2. Material and methods

2.1. Materials

A novel low-cost adsorbent, iron oxide on activated alumina, was developed as follows [22]. The activated alumina grains were sieved before seeding and then packed into the 30 m^3 FBR (2.1 m Ø × 9 m height). The internal circulation of the FBR was controlled to maintain an upflow superficial velocity of 40 m h^{-1} with a 50% bed expansion. The bioeffluent of tannery wastewater, H_2O_2 and $FeSO_4$ were fed continuously into the bottom of the reactor. The molar ratio of H_2O_2 to $FeSO_4$ was 3.2:1. The pH of the solution, which was adjusted by adding dilute aqueous solutions of NaOH or H_2SO_4, was maintained at 3, to prevent the precipitation of $Fe(OH)_3$ [19]. The crystals were grown onto the surface of the activated alumina grains, i.e. F1 adsorbent for 3 months. The color of activated alumina particles changed from silvery white to brown after crystallization. The crystallized grains were washed with tap water and were taken out from the FBR. The finial grains were dried at room temperature for 120 h before the application. The aqueous stock solution of copper ($Cu(NO_3)_2$, Riedel-de Haën) was prepared using deionized water (Millipore Milli-Q).

2.2. Characterization of the adsorbent

The physico-chemical characteristics of the F1 adsorbent were elucidated using standard procedures. The Brunauer–Emmett–Teller (BET) surface area and porosity of the adsorbents were obtained from the isotherms. The surface area of the adsorbents was calculated from the BET equation. X-ray diffraction (XRD) and scanning electron microscopy (SEM) of the adsorbent were conducted. XRD powder diffraction of the adsorbent was performed using a powder diffractometer (Rigaku RX III) with Cu Kα radiation. The accelerating voltage and current were 40 kV and 20 mA. The morphology of the adsorbent was described using a Hitachi S-4100 SEM.

2.3. Batch experimental program

0.2 g of adsorbent was added to each of various solutions with initial Cu^{2+} concentrations from 0.1 to 0.8 mM (100 ml, pH 6.0), to evaluate the thermodynamic properties. These samples were then mounted on a shaker and shaken continuously for 24 h at 288, 308 and 318 K. Solutions pH were controlled at 6.0 ± 0.05 by adding dilute HCl or NaOH solutions during the whole experiments. The suspensions were filtered using a 0.25 μm syringe filter made of poly-(vinylidene fluoride) membrane, and the filtrates were immediately measured by atomic absorption spectroscopy (Hitachi Z-6100). The differences between the initial and the equilibrium Cu^{2+} concentrations determine the amount of Cu^{2+} that is adsorbed by the adsorbent.

The kinetic of adsorption experiment involved the Jar Test at a constant speed of 150 revolutions per minutes (rpm). The samples were prepared by adding 5 g of adsorbent to 1000 ml solution (pH 6.0); the Cu^{2+} concentrations were 0.1, 0.2, 0.4 and 0.8 mmol l^{-1} at 300 ± 1 K. The amount of sorbed metal per gram of adsorbent q_t at time t was determined as follows [23]:

$$q_t = \frac{C_0 - C_t}{m_{\text{ads}}}, \quad (1)$$

where C_0 is the initial Cu^{2+} concentration of the liquid phase at and C_t is that at any time t (in mg l^{-1}); m_{ads} is the amount of adsorbent in the solution (g l^{-1}).

3. Results and discussion

3.1. Characterization of the adsorbent

Table 1 presents the characteristics of the F1 adsorbent. Fig. 1 displays the morphology of the original activated alumina grain support (Fig. 1a) and the F1 adsorbent (Fig. 1b). Comparing Fig. 1a with Fig. 1b reveals that the morphology was smoother after the reaction in the FBR had proceeded for 3 months. Fig. 2 shows the XRD patterns of the F1 adsorbent. The XRD data were analyzed using the F1 adsorbent of iron according to the diffraction files of the Joint Committee on Powder Diffraction Standards (JCPDS). The JCPDS data on oxyhydroxides of iron were compared. The main diffraction peaks of the F1 adsorbent at $2\theta = 21.2°$, 36.6° and 53.2° were carefully com-

Table 1
Properties of the F1 adsorbent

Parameter	Value
Material of support	Al_2O_3
Total iron content of iron oxide (g kg^{-1})	304
Bulk density (g cm^{-3})	1.43
Absolute (true) density (g cm^{-3})	2.66
Specific surface area (m^2 g^{-1})	170
Total pore volume (cm^3 g^{-1})	0.12
Average particle size (mm)	0.39

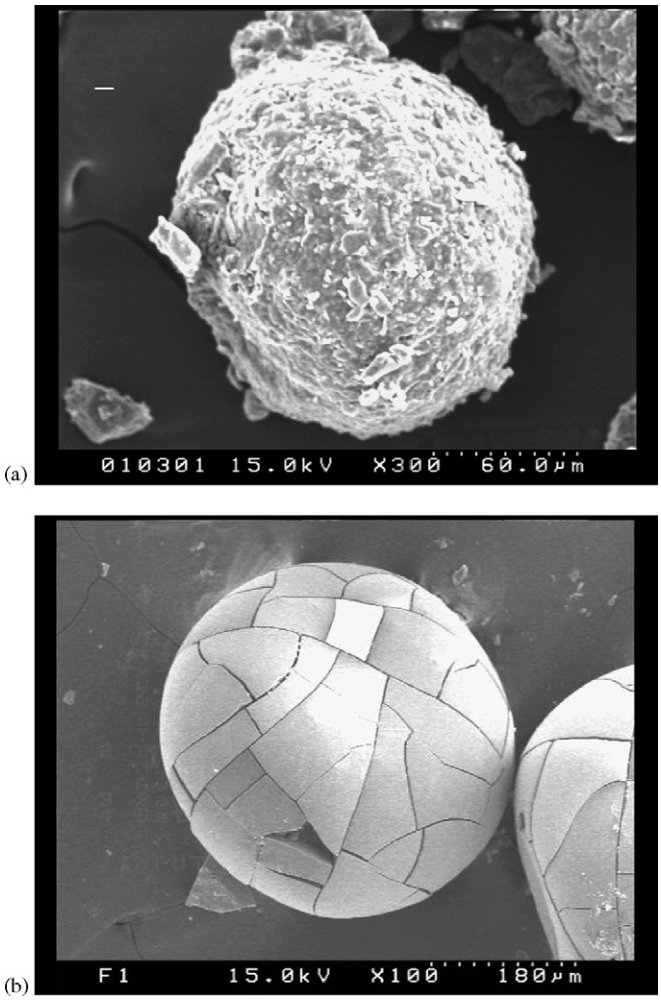

Fig. 1. Scanning electron micrographs of (a) original support and (b) F1 adsorbent.

pared with the standard for goethite (α-FeOOH—file number 81-0464). Accordingly, the peaks of F1 adsorbent were identified with the phase α-FeOOH. However, the XRD pattern of the F1 adsorbent exhibits very weak diffraction intensities in the region $2\theta = 10$–80°, indicating that the F1 adsorbent contained a very small amount of crystalline goethite. The pH value associated with zero charge (pH_{pzc}) on the F1 adsorbent was around 7.35. More information on the method of measuring pH_{pzc} is available elsewhere [24].

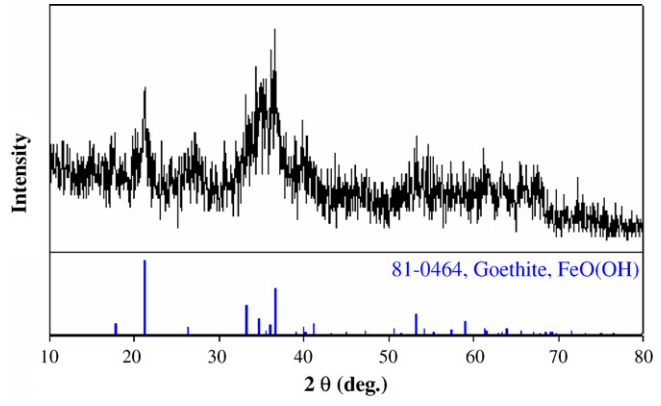

Fig. 2. X-ray diffraction pattern of the F1 adsorbent showing the intensities in the region $2\theta = 10$–80°.

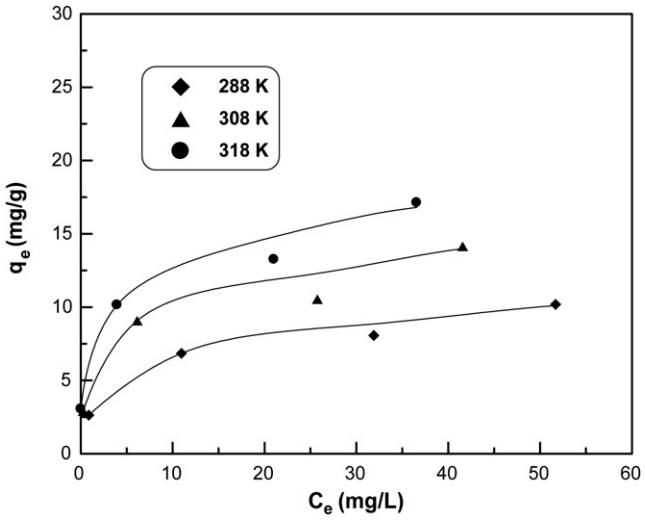

Fig. 3. Adsorption isotherms of Cu^{2+} onto F1 adsorbent at different temperatures.

3.2. Adsorption isotherm

Fig. 3 plots the adsorption isotherms of Cu^{2+} adsorption by F1 adsorbent at various temperatures. All batch experimental data were fitted to the isotherm models of the well-known Langmuir and Freundlich using the method of least squares and an optimization algorithm. There models are represented mathematically as follows.

The Langmuir isotherm model is obtained by combining the adsorption and desorption rate equations [23].

$$\frac{d\theta_t}{dt} = k_{ads} C_t N(1 - \theta_t) - k_d N \theta_t, \tag{2}$$

where N is the maximum number of adsorption sites occupied by the Cu^{2+} and θ_t is the dimensionless surface coverage ratio ($\theta_t = q_t/q_m$). When the sorption process reaches equilibrium, Eq. (2) yields

$$q_e = \frac{K_L q_m C_e}{1 + K_L C_e}, \tag{3}$$

where $K_L = k_{ads}/k_d$ is the Langmuir constant; q_m is the maximum adsorption capacity (mg g^{-1}) and q_e is the amount of Cu^{2+} sorbed at equilibrium (mg g^{-1}). Rearranging Eq. (3) yields the Langmuir parameters:

$$\frac{C_e}{q_e} = \frac{1}{K_L q_m} + \frac{C_e}{q_m}. \tag{4}$$

The Freundlich isotherm model show the relationship between the amount of Cu^{2+} adsorbed by the F1 adsorbent (q_e, mg g^{-1}) and the equilibrium concentration of Cu^{2+} (C_e, mg l^{-1}) in solution [25]:

$$q_e = K_F C_e^{1/n}, \tag{5}$$

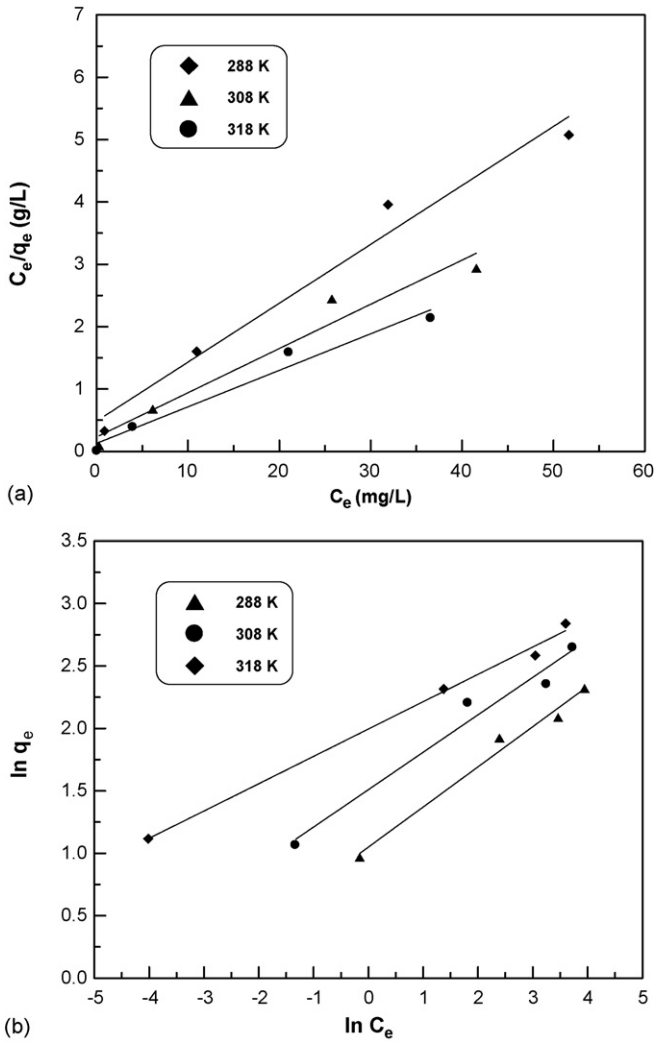

Fig. 4. Linearized (a) Langmuir and (b) Freundlich isotherm models for Cu^{2+} adsorption by the F1 adsorbent at different temperatures.

where K_F and n are Freundlich constants that are related to the adsorption capacity and adsorption intensity, respectively.

Fig. 4a and b displays linear plots of C_e/q_e versus C_e and $\ln q_e$ versus $\ln C_e$. For each isotherm in Fig. 4a, the values of q_m and K_L were determined from experimental data by linear regression. According to Fig. 4b, the values of K_F and n were obtained similarly. The data in Table 2 presents the results, along with associated correlation coefficients (R^2). The data in Table 2 reveals that the Freundlich model yields a better fit than the Langmuir model, according to the correlation coefficients at various temperatures.

Table 2
Parameters of Langmuir and Freundlich adsorption isotherm models for Cu^{2+} on F1 adsorbent

T (K)	Langmuir			Freundlich		
	q_m	K_L	R^2	K_F	n	R^2
288	10.58	0.1946	0.9744	2.854	3.107	0.9834
308	14.10	0.3082	0.9585	4.525	3.336	0.9710
318	17.08	0.4564	0.9714	7.355	4.569	0.9944

The Cu^{2+} adsorption capacity increases with temperature, indicating that the reaction is endothermic. Thermodynamic parameters can be determined from the variation of the thermodynamic equilibrium constant K_0 with temperature [25,26]. For adsorption reactions, K_0 is defined as follows:

$$K_0 = \frac{a_s}{a_e} = \frac{v_s}{v_e}\frac{C_s}{C_e}, \tag{6}$$

where a_s is the activity of adsorbed Cu^{2+}; a_e is the activity of the Cu^{2+} in solution at equilibrium; C_s is the surface concentration of Cu^{2+} (mmol g^{-1}) in the exchanger; C_e is the Cu^{2+} concentration in solution at equilibrium (mmol ml^{-1}); v_s represents the activity coefficient of the adsorbed Cu^{2+}; v_e is the activity coefficient of the Cu^{2+} in solution. As the Cu^{2+} concentration in the solution declines to zero, K_0 can be obtained by plotting $\ln(C_s/C_e)$ versus C_s (Fig. 5) and extrapolating C_s to zero [25,26]. The straight line obtained is fitted to the points by least-squares analysis. Its intercept with the vertical axis yields the values of K_0. The adsorption standard free energy changes (ΔG°) can be calculated from

$$\Delta G^\circ = -RT \ln K_0, \tag{7}$$

where R is the universal gas constant (8.314 J mol^{-1} K^{-1}) and T is the temperature in Kelvin. The average standard enthalpy change (ΔH°) is determined from the Van't Hoof equation,

$$\ln K_0(T_3) - \ln K_0(T_1) = \frac{-\Delta H^\circ}{R}\left(\frac{1}{T_3} - \frac{1}{T_1}\right), \tag{8}$$

where T_3 and T_1 are different temperatures. The standard entropy change (ΔS°) is given by

$$\Delta S^\circ = -\frac{\Delta G^\circ - \Delta H^\circ}{T}, \tag{9}$$

Table 3 presents the thermodynamic parameters. Additionally, Fig. 6 plots the free energy change versus enthalpy change to

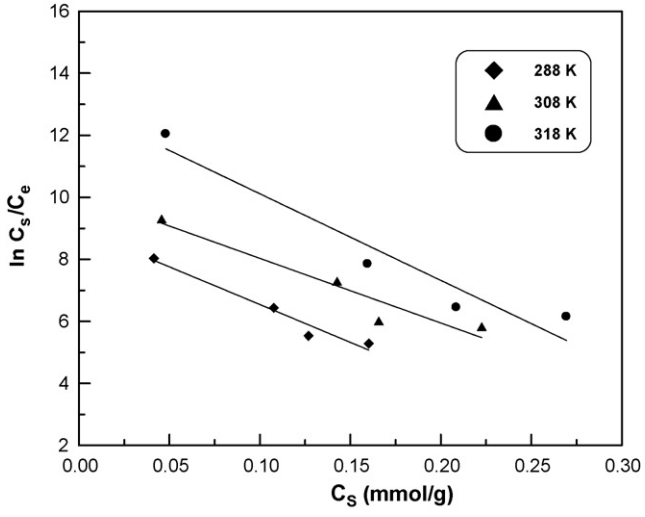

Fig. 5. Plots of $\ln(C_s/C_e)$ vs. C_s at various temperatures.

Table 3
Values of various thermodynamic parameters for adsorption of Cu^{2+} on F1 adsorbent

Thermodynamic constant	Temperature (K)		
	288	308	318
K_0	8.98	10.12	12.91
ΔG° (kJ mol^{-1})	−5.25	−5.53	−6.12
ΔH° (kJ mol^{-1})	9.20	9.20	9.20
ΔS° (J mol^{-1} K^{-1})	50.20	47.86	48.19

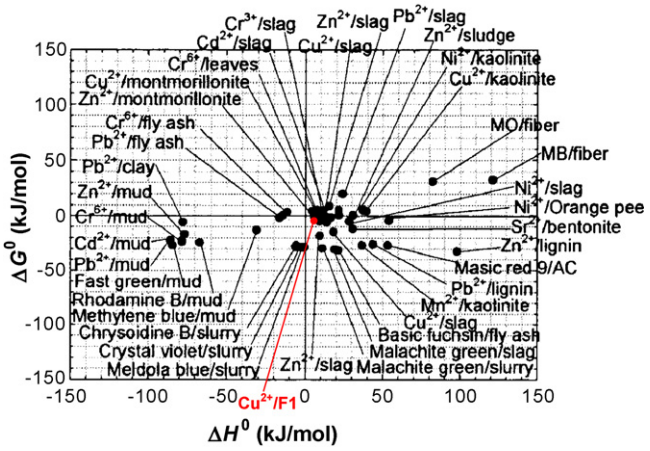

Fig. 6. The standard free energy change vs. standard enthalpy change for F1 adsorbent and the other adsorption systems investigated in previous literature [27].

yield the thermodynamic parameters evaluated herein and previous literature [27]. A positive standard enthalpy change of 9.2 kJ mol^{-1} obtained in this study indicates that the adsorption of Cu^{2+} by the F1 adsorbent is endothermic, which fact is evidenced by the increase in the adsorption of Cu^{2+} with temperature. A negative change in adsorption standard free energy reveals that the adsorption reaction is a spontaneous process [25,26]. The positive standard entropy change may be caused the release of water molecules in the ion exchange reaction between the adsorbate and the functional groups on the surfaces of the F1 adsorbent. These results were similar to most of the data shown in Fig. 6. In previous literature, although the standard enthalpy

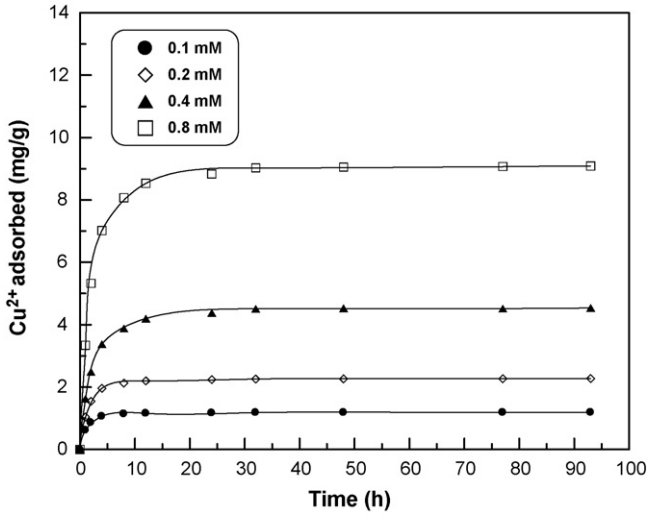

Fig. 7. Effect of contact time on Cu^{2+} adsorption rate for different concentrations (pH 6.0, at 300 ± 1 K).

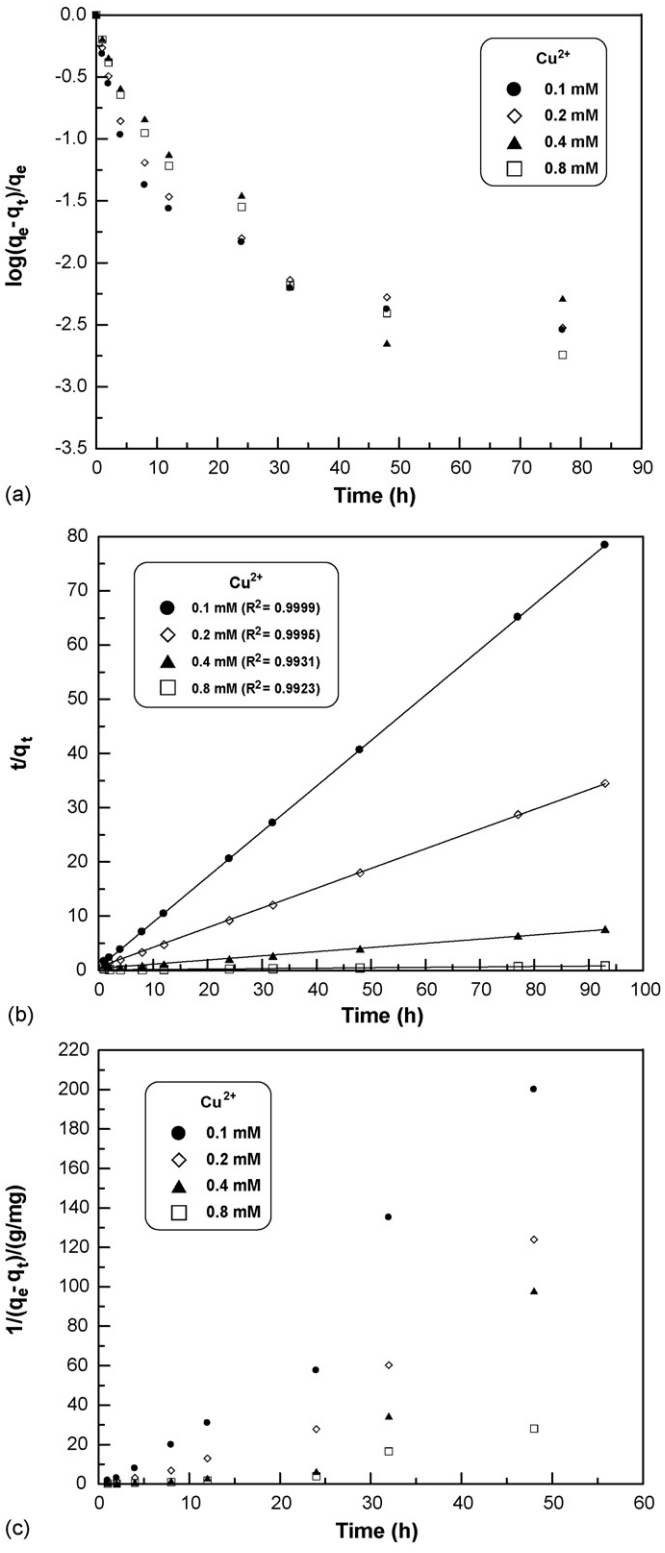

Fig. 8. Test of (a) the first-order Lagergren, (b) the pseudo-second-order and (c) the second-order rate equation for adsorption of different concentrations of Cu^{2+} by F1 adsorbent (pH 6.0, at 300 ± 1 K).

change for adsorption of very different adsorbate onto distinct adsorbent covers a wide range (−85 to +160 kJ mol^{-1}), the standard free energy change at 30 °C remain within ±30 kJ mol^{-1}. Restated, the enthalpy and entropy contributions for driving the adsorption process are largely compensated each other for very different adsorbate/adsorbent systems. This phenomenon needs further investigation since if it were correct, the reason why a universal correlation could exist between the corresponding enthalpy change and entropy change following adsorption remains unclear [27].

3.3. Kinetics of adsorption

The adsorption kinetics, yielding the solute uptake rate, are the most important determinant of the adsorption efficiency of the F1 adsorbent and therefore, its potential application. Fig. 7 presents the effect of the contact time on the Cu^{2+} adsorption rate for various concentrations. According to Fig. 7, the Cu^{2+} adsorption rates increase dramatically during the first 12 h at various initial concentrations, reaching equilibrium slowly at 24 h. The first-order Lagergren equation (10), the pseudo-second-order rate equation (11) and the second-order rate equation (12) were evaluated from the experimental data to evaluate the rate of adsorption of Cu^{2+} onto the F1 adsorbent [28],

$$\log\left(\frac{q_e - q_t}{q_e}\right) = -\frac{k_L t}{2.3}, \tag{10}$$

$$\frac{t}{q_t} = \frac{1}{2k' q_e^2} + \frac{t}{q_e}, \tag{11}$$

$$\frac{1}{q_e - q_t} = \frac{1}{q_e} + kt, \tag{12}$$

where k_L is the Lagergren rate constant of adsorption (h^{-1}); k' is the pseudo-second-order rate constant of adsorption (g mg^{-1} h^{-1}); k is the rate constant (g mg^{-1} h^{-1}); q_e and q_t are the amounts of metal ion sorbed (mg g^{-1}) at equilibrium and at time t, respectively. Fig. 8a–c plots $\log(q_e - q_t)/q_e$ versus t, t/q_t versus t and $1/(q_e - q_t)$ versus t. These figures clearly indicate that the pseudo-second-order rate equation yields the best fit and the correlation coefficients of the pseudo-second-order rate model for the linear plots are very close to 1 at various concentrations (Fig. 8b), suggesting that kinetic adsorption can be described by the pseudo-second-order rate equation.

4. Conclusion

The surface of the F1 adsorbent was characterized by XRD and was identified as α-FeOOH. Additionally, the ability of F1 adsorbent to bind Cu^{2+} was investigated with reference to equilibrium, kinetics and thermodynamics.

Langmuir and Freundlich adsorption isotherm models were employed to describe the Cu^{2+} adsorption to F1 adsorbent at various temperatures. The Freundlich model fits the experimental data better than does the Langmuir model. Furthermore, a positive standard enthalpy change suggests that the adsorption of Cu^{2+} by F1 adsorbent is endothermic. The negative adsorption standard free energy changes reveal that the adsorption reaction is spontaneous. The pseudo-second-order rate model accurately describes the kinetics of adsorption.

Acknowledgement

The authors would like to thank the National Science Council of the Republic of China, Taiwan, for financially supporting this research under Contract No. NSC 94-2211-E-006-032.

References

[1] C.O. Adewunmi, W. Becker, O. Kuehnast, F. Oluwole, G. Dörfler, Sci. Total Environ. 193 (1996) 69.
[2] S. Al-Asheh, F. Banat, Environ. Geol. 40 (2001) 693.
[3] M. Lehmann, A.I. Zouboulis, K.A. Matis, Chemosphere 39 (1999) 881.
[4] D. Ghosh, K.G. Bhattacharyyra, J. Appl. Clay Sci. 20 (2002) 295.
[5] M.J.S. Yabe, E. Oliveira, Adv. Environ. Res. 7 (2003) 263.
[6] A. Netzer, D.E. Hughes, Water Res. 18 (1984) 927.
[7] M.O. Corapcioglu, C.P. Huang, Water Res. 21 (1987) 1031.
[8] T.K. Budinova, K.M. Gergova, N.V. Petrov, V.N. Minkova, J. Chem. Technol. Biotechnol. 60 (1994) 177.
[9] M. Machida, M. Aikawa, H. Tatsumoto, J. Hazard. Mater. 120 (2005) 271.
[10] S. Akhtar, R. Qadeer, Adsorpt. Sci. Technol. 15 (1997) 815.
[11] Y.S. Ho, G. McKay, Process Biochem. 34 (1999) 451.
[12] S. Babel, T.A. Kurniawan, J. Hazard. Mater. 97 (2003) 219.
[13] S.E. Bailey, T.J. Olin, R.M. Bricka, D.D. Adrian, Water Res. 33 (1999) 2469.
[14] B.B. Johnson, Environ. Sci. Technol. 24 (1990) 112.
[15] Manceau, L. Charlet, J. Colloid Interf. Sci. 168 (1994) 87.
[16] S. Fendorf, M.J. Eick, P. Grossl, D.L. Sparks, Environ. Sci. Technol. 31 (1997) 315.
[17] P. Venema, T. Hiemstra, P.G. Weidler, W.H. Van Riemsdijk, J. Colloid Interf. Sci. 198 (1998) 252.
[18] S.G.J. Heijman, A.M. Paassen, W.G.J. Meer, R. Hopman, Water Sci. Technol. 40 (1999) 183.
[19] S. Chou, C. Huang, Y.H. Huang, Chemosphere 39 (1999) 1997.
[20] S. Chou, C. Huang, Y.H. Huang, Environ. Sci. Technol. 35 (2001) 1247.
[21] C.L. Hsueh, Y.H. Huang, C.Y. Chen, J. Hazard. Mater. 129 (2006) 228–233.
[22] Y.H. Huang, G.H. Huang, S. Chou, H.S. Perng, USA patent, US6143182 (2000).
[23] N. Chiron, R. Guilet, E. Deydier, Water Res. 37 (2003) 3079.
[24] W. Stumm, Chemistry of the Solid–Water Interface, Wiley/Interscience, New York, 1992.
[25] Y.H. Li, Z. Di, J. Ding, D. Wu, Z. Luan, Y. Zhu, Water Res. 39 (2005) 605.
[26] R. Niwas, U. Gupta, A.A. Khan, K.G. Varshney, Colloids Surf. A: Physicochem. Eng. Aspects 164 (2000) 115.
[27] A. Ramesh, D.J. Lee, J.W.C. Wong, J. Chin. Inst. Chem. Eng. 3 (2005) 203.
[28] B. Benguella, H. Benaissa, Water Res. 36 (2002) 2463.